LASER INTERFEROMETER GRAVITATIONAL WAVE OBSERVATORY
- LIGO -
CALIFORNIA INSTITUTE OF TECHNOLOGY
MASSACHUSETTS INSTITUTE OF TECHNOLOGY

Technical Note	LIGO-T080186-01-I	2009/03/14
Modeling of Alignment Sensing and Control for Enhanced LIGO		
L. Barsotti, M. Evans		

This is an internal working
note of the LIGO project

California Institute of Technology
LIGO Project, MS 18-34
Pasadena, CA 91125
Phone (626) 395-2129
Fax (626) 304-9834
E-mail: info@ligo.caltech.edu

Massachusetts Institute of Technology
LIGO Project, Room NW17-161
Cambridge, MA 02139
Phone (617) 253-4824
Fax (617) 253-7014
E-mail: info@ligo.mit.edu

LIGO Hanford Observatory
Route 10, Mile Marker 2
Richland, WA 99352
Phone (509) 372-8106
Fax (509) 372-8137
E-mail: info@ligo.caltech.edu

LIGO Livingston Observatory
19100 LIGO Lane
Livingston, LA 70754
Phone (225) 686-3100
Fax (225) 686-7189
E-mail: info@ligo.caltech.edu

WWW: http://www.ligo.caltech.edu/

Abstract

This note presents a model of the alignment sensing and control (ASC) for Enhanced LIGO based on the Optickle simulation tool. In particular, effects induced by the radiation pressure are studied and discussed.

1 Introduction

Sensing and controlling the angular degrees of freedom of the mirrors is one of the main challenges in operating a gravitational wave interferometer at high power. The radiation pressure produced by the light circulating inside the IFO affects the response of the mirror suspension, in some cases destabilizing the mechanical system.

In initial LIGO (iLIGO) the power entering the IFO was about 6 W, with a power stored inside the Fabry-Perot cavities of about 20 kW. The optical torques induced on the test masses by the radiation pressure were still weak enough that they could be compensated by the auto-alignment system without significantly affecting the performance of the IFO.

For enhanced LIGO (eLIGO) the incoming power is 35 W, about a factor 6 bigger, with an intracavity power around 120 kW. As it will be detailed in the next section, the statically unstable mode of the optical spring will largely dominate the restoring torque of the mirror suspension. The most direct way of compensating for the optical spring is increasing the bandwidth of the auto-alignment system. However, the obvious drawback of this solution is the consequent increasing of the angular control noise, which must remain significantly below the sensitivity goal.

The analysis which follows is based on the frequency domain tool Optickle [1], in which angular transfer functions are computed taking into account radiation pressure effects.

2 Optical torques in eLIGO

The analysis of optical toques in suspended Fabry-Perot interferometers, and in particular in the iLIGO and advLIGO Fabry-Perot cavities, has been addressed in [2]. It is trivial to extend the results presented there to the eLIGO Fabry-Perot cavities. In the quasi-static approximation, a torsional stiffness matrix which couples to the angular displacement of the two cavity mirrors (α_{ETM} and α_{ITM}) is defined in terms of the g factors of the cavity:

$$\mathbf{k} = -\frac{2PL}{c(1 - g_1 g_2)} \begin{bmatrix} g_2 & 1 \\ 1 & g_1 \end{bmatrix}$$

where P is the intracavity power, L is arm cavity length and c is the speed of light.

Parameter	Value
P (intracavity power)	120 kW
L (arm cavity length)	4 km
g1 (g factor ETM)	0.460
g2 (g factor ITM)	0.726

Table 1: eLIGO parameters

With the eLIGO parameters reported in table 1 the two eigenvalues of the matrix $\mathbf{k}$ are:

$$k\_stable = 2.05 \tag{2.1}$$
$$k\_unstable = -7.86 \tag{2.2}$$

They correspond to the stable and unstable mode of the cavity:

$$\overrightarrow{v}\_stable = 0.876\, \widehat{\alpha}_{ETM} - \widehat{\alpha}_{ITM} \tag{2.3}$$
$$\overrightarrow{v}\_unstable = \widehat{\alpha}_{ETM} + 0.876\, \widehat{\alpha}_{ITM} \tag{2.4}$$
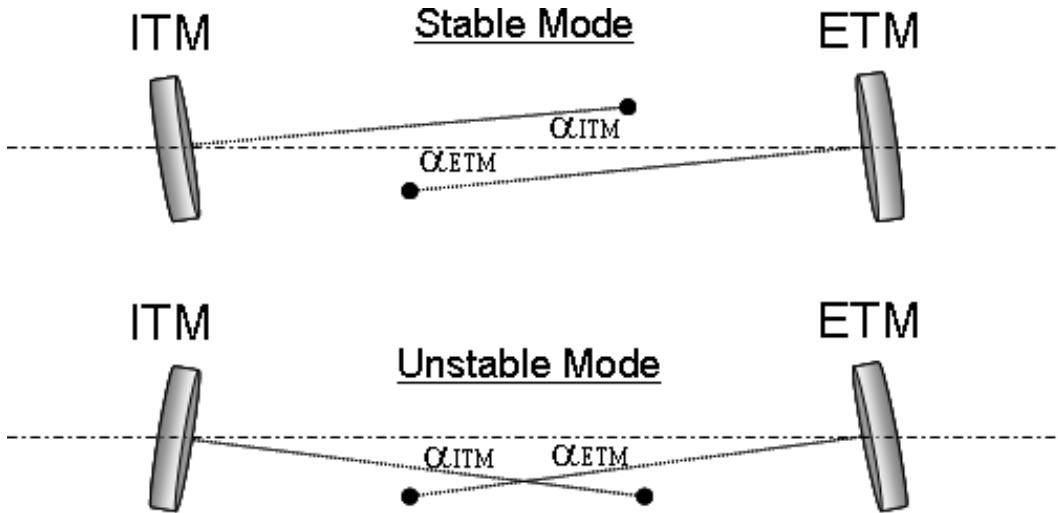

Figure 1: Statically stable and unstable modes of a single cavity in presence of radiation pressure.

The restoring torque of the pendulum is about 0.5 Nm, not enough to compensate for the unstable mode torque k_unstable, which is about 15 times bigger.

3   Modification of the angular transfer functions of the eLIGO mirror induced by radiation pressure

The input power entering the eLIGO IFO is $P_{in} = 35$ W and the power stored inside each Fabry-Perot cavity is about 120 kW. Optickle computes transfer functions only for pitch, but equivalent results are expected for yaw. Figure 2 shows how the simple pendulum mechanical transfer function of the different mirrors is modified by radiation pressure. As expected, the PR transfer function is slightly modified, and the resonance frequency remains the same. In the transfer functions of the input and end mirrors (ITMs and ETMs) the 0.5 Hz pitch resonance is instead shifted to higher frequency.
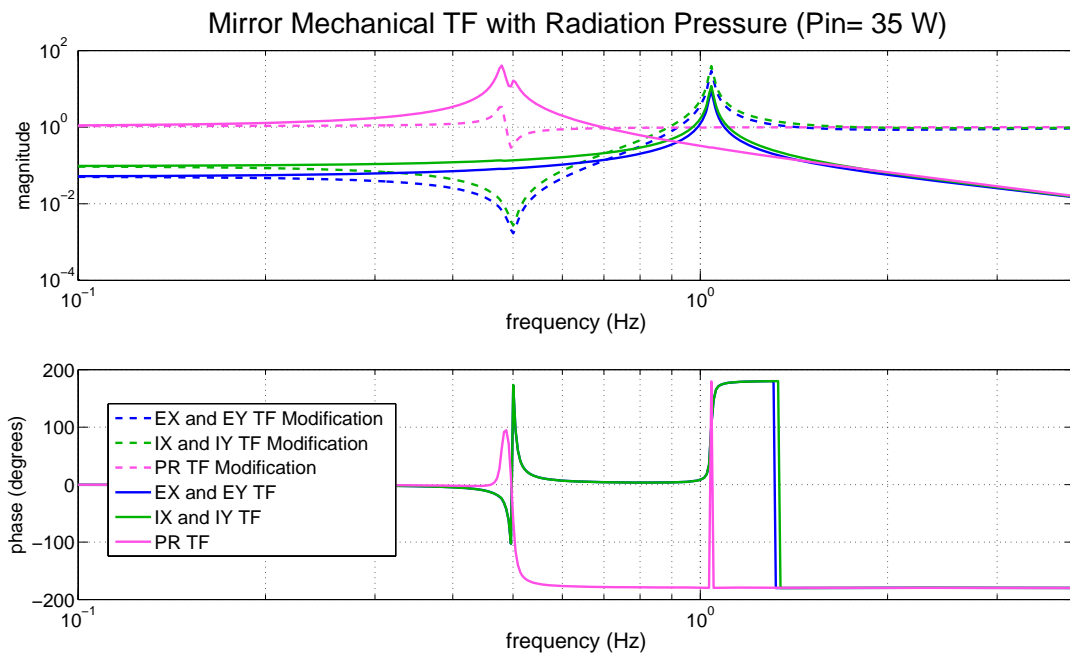

Figure 2: Mechanical transfer function of ITMS, ETMs and PR with an input power of 35 W and an intracavity power of about 120 kW. Dotted lines correspond to the modifications to the pendulum transfer function induced by radiation pressure, the continue lines are the corresponding modified pendulum transfer functions.

The basis which diagonalizes the matrix of the mechanical transfer functions in presence of radiation pressure is not the mirror basis, but, as suggested in the previous section and confirmed by the Optickle model, the common and differential combination of the unstable and stable modes of the two arm cavities:

$$\text{CommUnstab} = (EX + EY) + r * (IX + IY) \tag{3.1}$$
$$\text{CommStable} = r * (EX + EY) - (IX + IY) \tag{3.2}$$
$$\text{DiffUnstab} = (EX - EY) + r * (IX - IY) \tag{3.3}$$
$$\text{DiffStable} = r * (EX - EY) - (IX - IY) \tag{3.4}$$

The factor r according to the Optickle model within 5% agreement with the theoretical value of 0.876. The digonalization of the matrix in this new basis is frequency and input power independent. Figure 3 shows the mechanical transfer functions in the new basis: the pendulum resonance in the stable modes is shifted to higher frequency (from 0.5 Hz to 1.25 Hz), whereas the unstable mode transfer functions experience a 360 degree phase loss at the 0.5 Hz pendulum resonance.
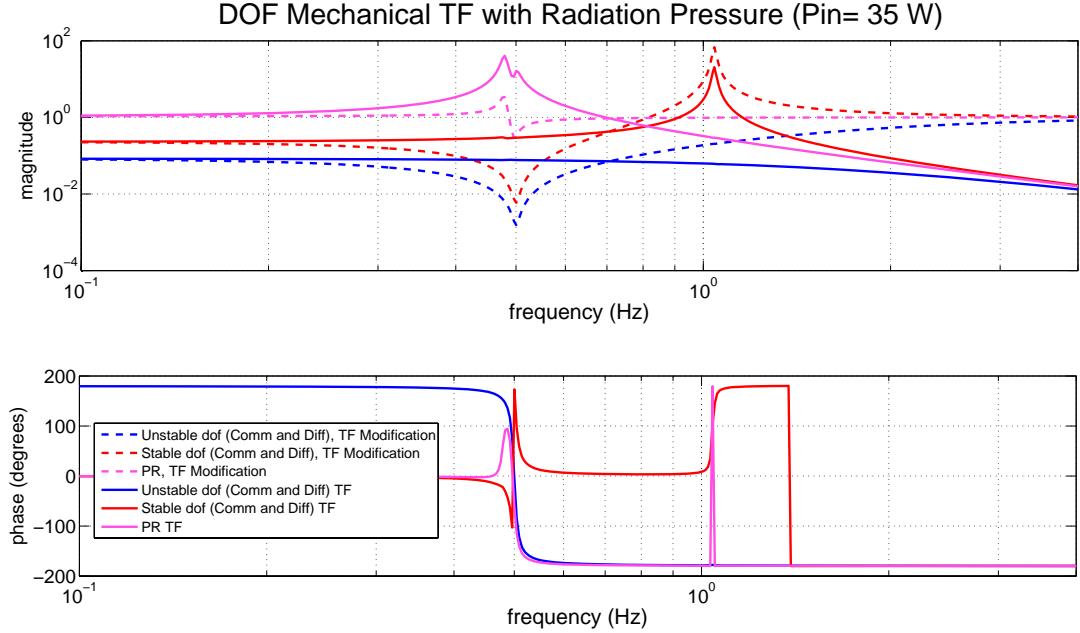

Figure 3: Mechanical transfer function of the common and differential dof, with an input power of 35 W and an intracavity power of about 120 kW.

4 Angular sensing matrix

The eLIGO parameters used in this model are described in [1]. In particular, the DC readout of gravitational waves at the AS port is implemented with a 20 pm offset in the differential end mirrors longitudinal position (DARM). In order to find a good set of signals able to reconstruct the 5 angular dofs of the IFO, we put two wave front sensors (WFSs) at different
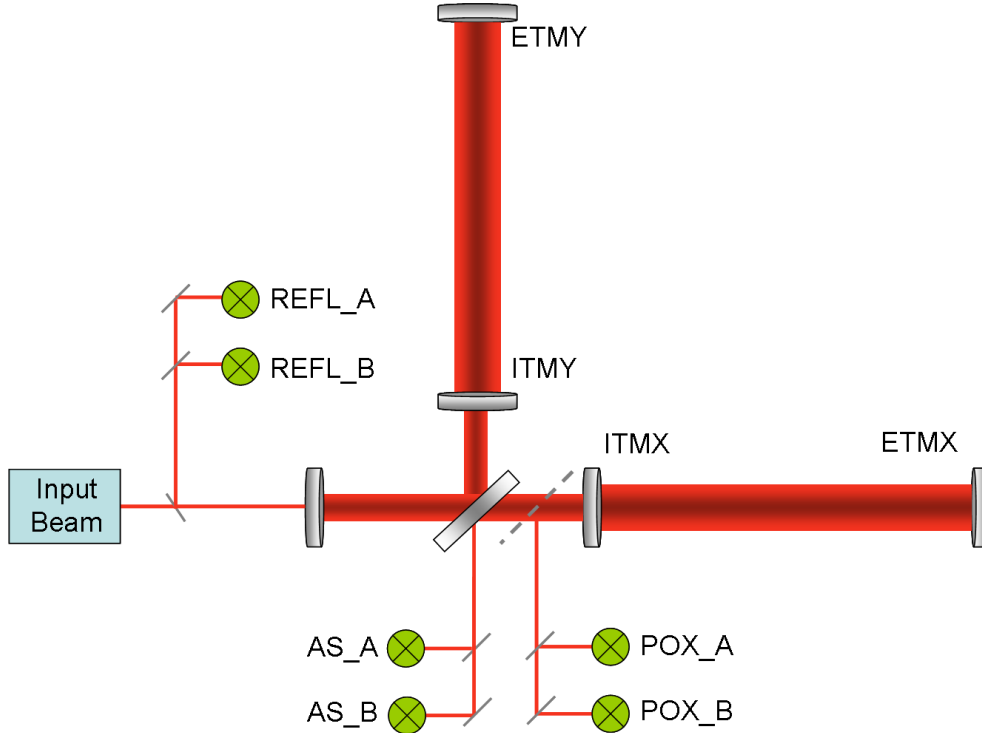
Figure 4: Simplified scheme of the eLIGO layout.

Gouy phases at the IFO output ports REFL, POX and AS (see figure 4). The two WFSs for each port will be identified by the suffix A and B.

The light entering the IFO is modulated at two radio frequencies $f_1 = 24.5$ MHz and $f_2 = 61$ MHz: f_1 is resonant in the recycling cavity and anti-resonant in the arms, f_2 is off-resonant in the recycling cavity. All the dofs of the IFO are reconstructed by demodulation, at the modulation frequencies f_1 or f_2, of the extracted signals. For each sensor, we have at least 4 signals available: I1, Q1 and I2, Q2. A sub-set of signals which allow the reconstruction of all 5 dofs are selected. Demodulation phases and Gouy phases are tuned in order to maximize the response of each signal to a given dof with respect to the other dofs. Consistent values of the demodulation phases are found by adopting a simpler procedure, which corresponds more directly to the experimental one: for each sensor, the sensitivity to a given dof is maximized on one of the two quadratures of the signal. At 10 Hz, the sensitivity of some of the available signals computed in Optickle is shown in table 2. For each sensor, the demodulation phases and Gouy phases are reported in table 3.

According to this model, two different WFSs need to be used at the REFL port, about at 90 degree Gouy phase apart, in order to have a good reconstruction both of the CommUstab dof and the PR dof. The other dofs, instead, can be reconstructed with only one WFS at the POX and AS ports. By normalizing the two phases of each signal for the maximum element, and zeroing the elements which are smaller than 10% the maximum one, we get the matrix shown in table 4. The signals which reconstruct all 5 angular dofs are shown in table 5, where each row is normalized by its maximum value.

	CommUnst	CommStab	DiffUnst	DiffStab	PR
REFL_B I2	-988.54	-299.85	-31.31	46.68	384.49
REFL_B Q2	-10.99	-3.34	-0.80	1.01	4.60
POX_A I1	-983.52	1169.8	-88.91	-0.01	1145.2
POX_A Q1	-49.34	71.02	-151.68	208.89	69.39
AS_A Q1	1655	-2073.2	16078	4905.4	-1887.8
AS_A I1	11.24	18.54	-0.51	-405.75	13.58
REFL_A I2	288.66	-1053	-49.23	48.23	-1460.2
REFL_A Q2	14.20	-3.55	-0.57	0.98	4.96

Table 2: Sensitivity of WFS signals to the angular dofs of the IFO computed in Optickle.

	Gouy phases (degrees)	Demod phases (degrees)
REFL_A	158	143.8
REFL_B	52	142.1
POX_A	135	173.0
AS_A	90	61.9

Table 3: Gouy phases of the sensors involved in the eLIGO sensing matrix and demodulation phases of the corresponding signals.

	CommUnst	CommStab	DiffUnst	DiffStab	PR
REFL_B I2	1	0.30	0	0	-0.39
REFL_B Q2	0	0	0	0	0
POX_A I1	0.84	-1	0	0	-0.98
POX_A Q1	0	0	0.13	-0.18	0
AS_A Q1	-0.10	0.13	-1	-0.31	0.11
AS_A I1	0	0	0	0	0
REFL_A I2	-0.20	0.72	0	0	1
REFL_A Q2	0	0	0	0	0

Table 4: Sensitivity of WFS signals to the angular dofs of the IFO computed in Optickle, normalized by the maximum element of the two phases of each signal.

	CommUnst	CommStab	DiffUnst	DiffStab	PR
REFL_B I2	1	0.30	0	0	-0.39
POX_A I1	0.84	-1	0	0	-0.98
POX_A Q1	-0.24	0.34	-0.73	1	0.33
AS_A Q1	-0.10	0.13	-1	-0.31	0.11
REFL_A I2	-0.20	0.72	0	0	1

Table 5: 5×5 sensing matrix used for the angular dof reconstruction normalized by the maximum element of each row.

4.1   Signals at the AS port

Because of the DARM offset implemented for DC readout, some carrier is transmitted at the AS port. The beating between the carrier and the sidebands resonant in the recycling cavity produces a signal sensitive to the differential angular dofs in both the phases of the demodulated signal. However, the matrix in table 4 shows that no significant sensitivity to any dof appears in the AS_A I1 signal. By increasing the DARM offset, the sensitivity to diffStab increases. However, in order to have an acceptable sensitivity (at least 10% of the sensitivity of AS_A Q1 to diffUnst), the DARM offset needs to be not smaller than 100 pm. Moreover, as shown in figure 5, the increasing of the DARM offset has the drawback of coupling AS_A Q1 to the common dofs. Having two WFSs at different Gouy phases at the AS port doesn't help either, as shown in figure 6.

The conclusion is that, even with DC readout, only one signal can be extracted at the AS port.
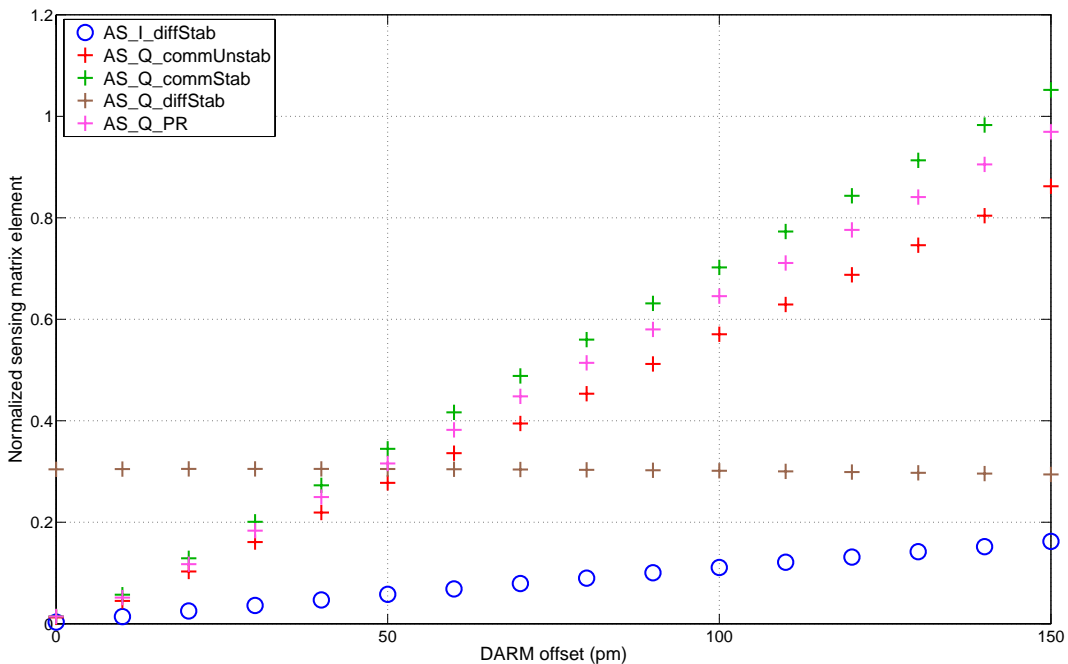

Figure 5: Elements of the AS sensing matrix plotted for different values of the DARM offset.

5   Tuning of the Gouy phases and demodulation phases

The tuning of the demodulation phases of the WFS signals in LIGO is done digitally, and a precision of fractions of 1 degree is easily achievable. On the other hand, a precise tuning of the WFS Gouy phases is much more difficult. It requires a very accurate knowledge of the optical layout of the IFO and the beam parameters in order to determine the position in which the WFS needs to be located. For this reason it is useful to know the sensitivity of the sensing matrix to variations of the Gouy phases from the optimal value. It turns out that the most sensitive Gouy phase is that of REFL_A. In order to have REFL_A I2 mostly sensitive to PR and not to CommUnstab, the Gouy phase needs to be not more than 10 degrees off.

Concerning the other WFSs, POX and AS, the sensing matrix does not change significantly (less than 20% in value, almost unchanged in ratios between the dofs) if the Gouy phases are tuned within 20 degrees with respect to the optimal value. The next plots (figures 6 7 8) show the sensitivity of the signals to the 5 dofs as function of the Gouy phase and the demodulation phase. The circles in the plots identify the Gouy phases and the demodulation phases as tuned in the Optickle model. Details about the way these plot are produced can be found in appendix B.
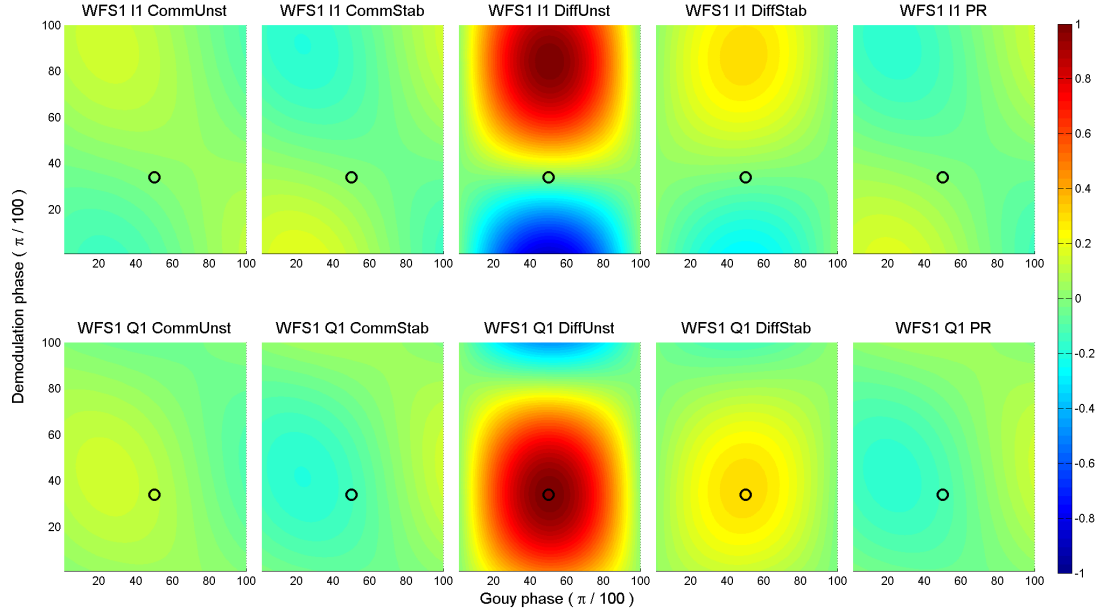

Figure 6: Sensitivity of the AS signals as function of the Gouy phase (x axis) and the demodulation phase (y axis).
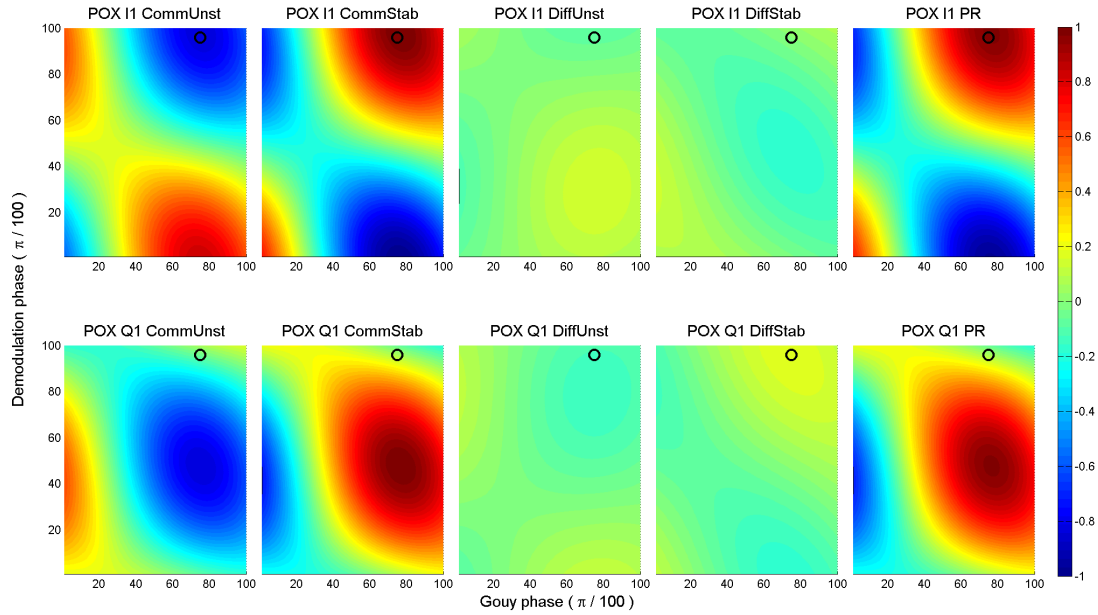
Figure 7: Sensitivity of the POX signals as function of the Gouy phase (x axis) and the demodulation phase (y axis).
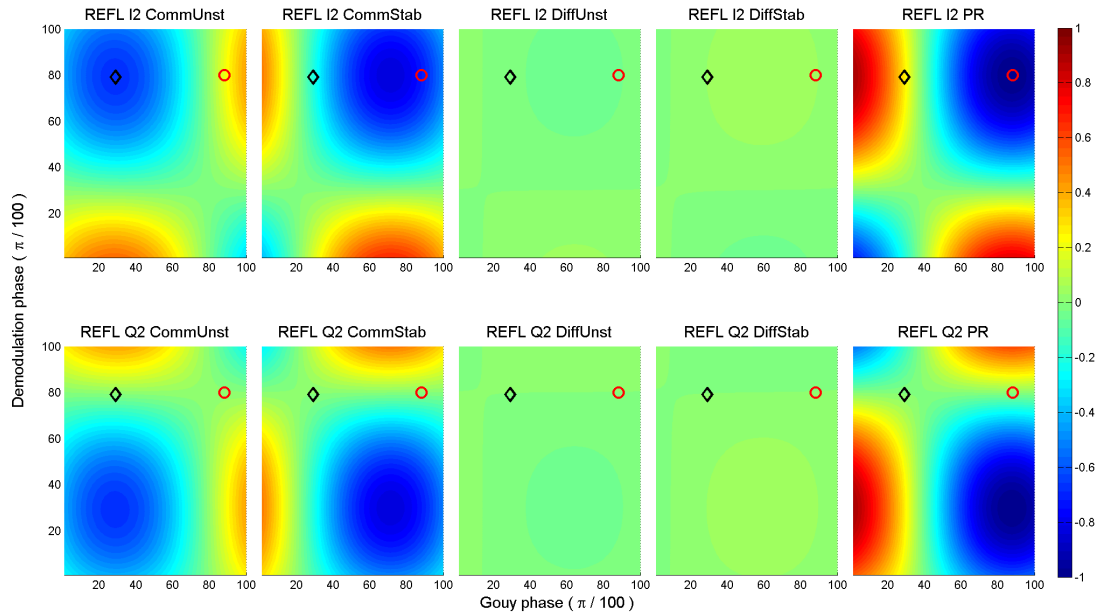

Figure 8: Sensitivity of the REFL signals as function of the Gouy phase (x axis) and the demodulation phase (y axis). The black diamond corresponds at the phase tuning of REFL_B (most sensitive to the common unstable dof), the red circle corresponds at the phase tuning of REFL_A (most sensitive to the PR dof).

6 Angular control loops

Control loops of the angular dofs are implemented in the model. By inverting the sensing matrix in table 5, all 5 angular dofs of the IFO can be reconstructed. Since the signal POX_A Q1 is the noisiest one, is used only for controlling the diffStab dof. Moreover, all the terms smaller than 30% have been neglected. The sensing matrix adopted in this model is therefore not exactly the matrix shown in table 5, but the one in table 6. The corresponding control matrix, normalized by the maximum element of each column, is shown in table 7.

	CommUnst	CommStab	DiffUnst	DiffStab	PR
REFL_B I2	1	0	0	0	-0.39
POX_A I1	0.84	-1	0	0	-0.98
AS_A Q1	0	0	-1	0	0
POX_A Q1	0	0	-0.73	1	0
REFL_A I2	0	0.72	0	0	1

Table 6: 5×5 sensing matrix used for the angular dof reconstruction normalized by the maximum element of each row.

	REFL_B I2	POX_A I1	AS_A Q1	POX_A Q1	REFL_A I2
CommUnst	0.35	0.28	0	0	0.39
CommStab	1	-1	0	0	-0.65
DiffUnst	0	0	-1	0	0
DiffStab	0	0	-0.73	-1	0
PR	-0.72	0.72	0	0	1

Table 7: Control matrix adopted in this model: the common dofs are controlled by using the signals REFL_B I2 , POX_A I1 and REFL_A I2, while the differential dofs are controlled by using AS_A Q1 and POX_A Q1.

The common dofs are sensed by using the signals REFL_B I2 , POX_A I1 and REFL_A I2, while the differential dofs are reconstructed by using AS_A Q1 and POX_A Q1.

6.1 The noises

The noise sources included in this model are the seismic noise due to the ground motion and the shot noise of the sensors.

6.1.1 Seismic noise

The attenuation of the seismic noise of the main optics in eLIGO is done as in iLIGO: the mirror is suspended by a simple pendulum hung on a mass-spring stack. A simple model of the angular pitch seismic noise of the mirrors is shown in plot 9. A typical horizontal ground motion measured at the LIGO sites (in blue) is filtered by the stack transfer function (Horizontal to horizontal, in red) and by the horizontal to pitch transfer function of the pendulum (in green). The model is compared with the angular seismic noise measured at the sites. The measurement has been done in iLIGO by inferring the angular motion of the mirror from the angular control signal needed to keep the optic in the aligned position [3]. The model and the real data agree quite well below a few Hz. Starting from 3 Hz the measured noise starts to be bigger than the expected one, with about a factor 1000 difference at 40 Hz. A possible reason for this discrepancy might be the noise reintroduced in the angular mirror position by the optical levers used for the angular stabilization of the mirror with respect to ground. Since no improvement is expected in the optical levers implemented in eLIGO, the measured angular seismic noise is used in this model.
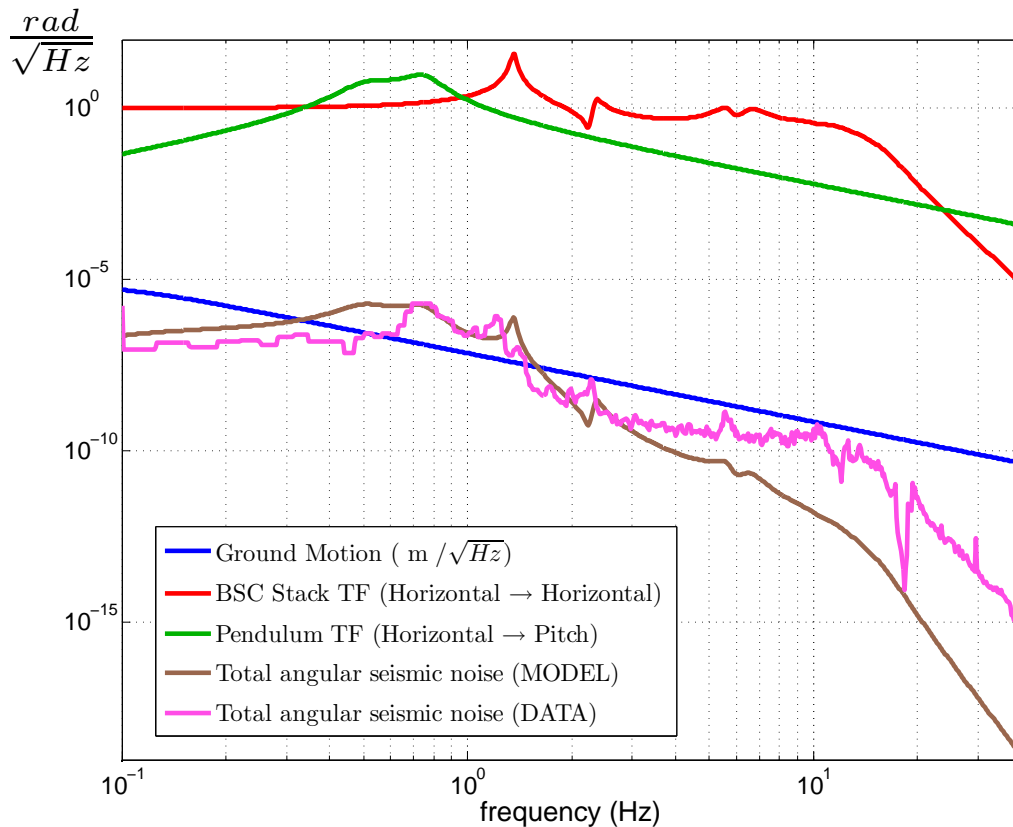

Figure 9: Angular seismic noise transferred to the mirrors as measured at the LIGO site (LHO, pink line). A model done by taking the measured ground motion (in blue) and filtering it by the stack TF (in red) and the pendulum TF (in green) largely differs from the measured spectrum starting at few Hz.

6.1.2 Shot noise

The shot noise of the sensors is computed with the usual formula:

$$\widetilde{P}_{shot} = \sqrt{2 \times h_P \times \nu \times P_{DC}} \quad W/\sqrt{Hz}$$

where h_P is the Plank's constant and $\nu = 2.8 \times 10^{14}$ Hz is the laser frequency.

The DC power P_{DC} is about **1 mW** on all the WFSs. In the model the WFSs are assumed to be shot noise limited and no other kind of sensing noise is included.

6.2 Control filters

The control filters used in this simulation compensate for the mechanical transfer function of the pendulum, and have high gain below 1 Hz in order to reduce the motion of the mirrors and a relatively strong cut-off around 20-30 Hz to prevent reintroduction of the sensor noise in the mirror position. Differences in the loop shapes are due to differences in the noise performance of sensors, as it will be more evident in the last section. The open loop transfer function and the closed loop transfer function for each dof is shown in figure 10 and figure 11. The unity gain frequencies of all the loops have been set to 6.5 Hz, except for the loops of the differential dofs: the unity gain frequency of the differential unstable loop is 10 Hz, the one of the the differential stable loop is 4 Hz. The phase margins of all the loops are around 30 degrees (except for the PR loop, which is about 40 Hz).

It is worth mentioning that a reduction of the unity gain frequency of the stable loops is possible without compromising the loop stability, with the only drawback of increasing the residual angular mirror motion. A reduction of the unity gain of the unstable dof loops is possible, but not by much as multiple crossings of the unity gain at low frequency are hard to prevent, and certainly unstable. The design of these filters is also quite critical: in the solution proposed here the gain margin is 2.

6.3 Residual angular mirror motion

In the hypothesis that seismic noise and shot noise are the main noise sources, the residual angular motion for each mirror is shown in figure 12. The RMS is around 5 nrad for the end mirrors, about a factor 2 bigger for the input mirrors. The plot shows the contribution from the seismic noise of the mirrors and the shot noise of the sensors.
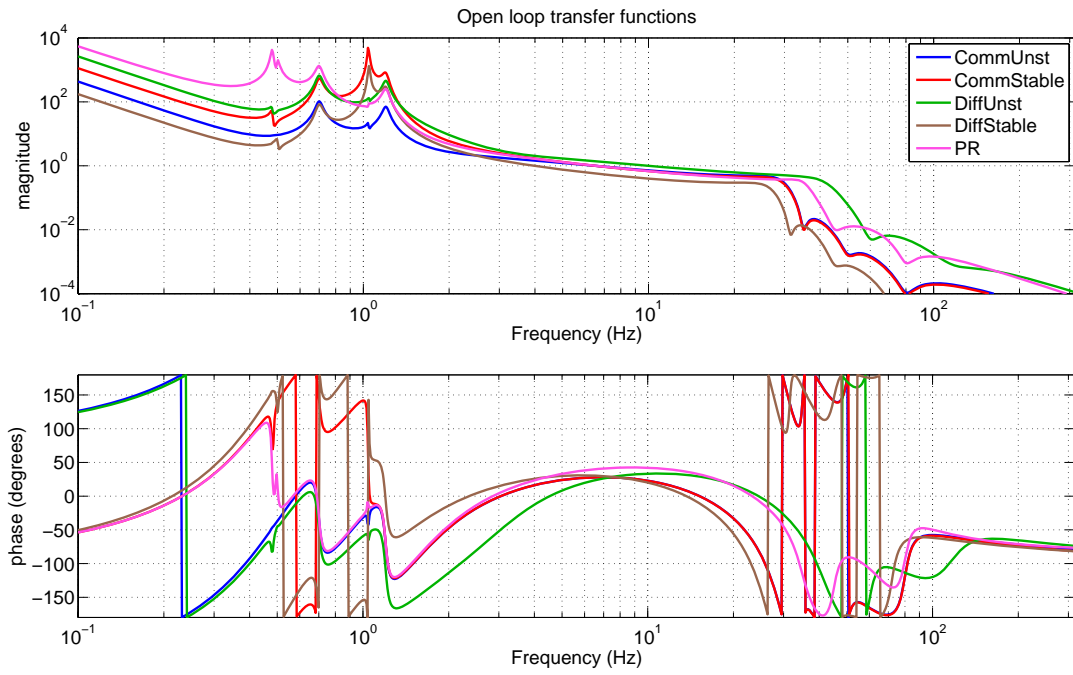
Figure 10: Open loop transfer function of the angular control system for each dof.
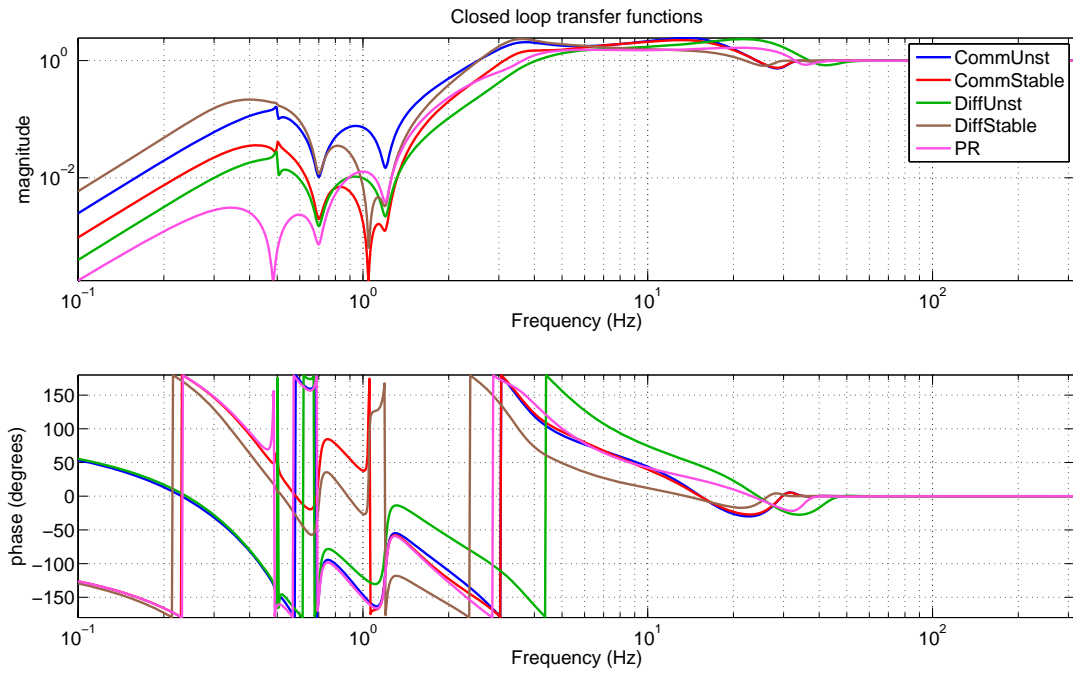

Figure 11: Closed loop transfer function of the angular control system for each dof.
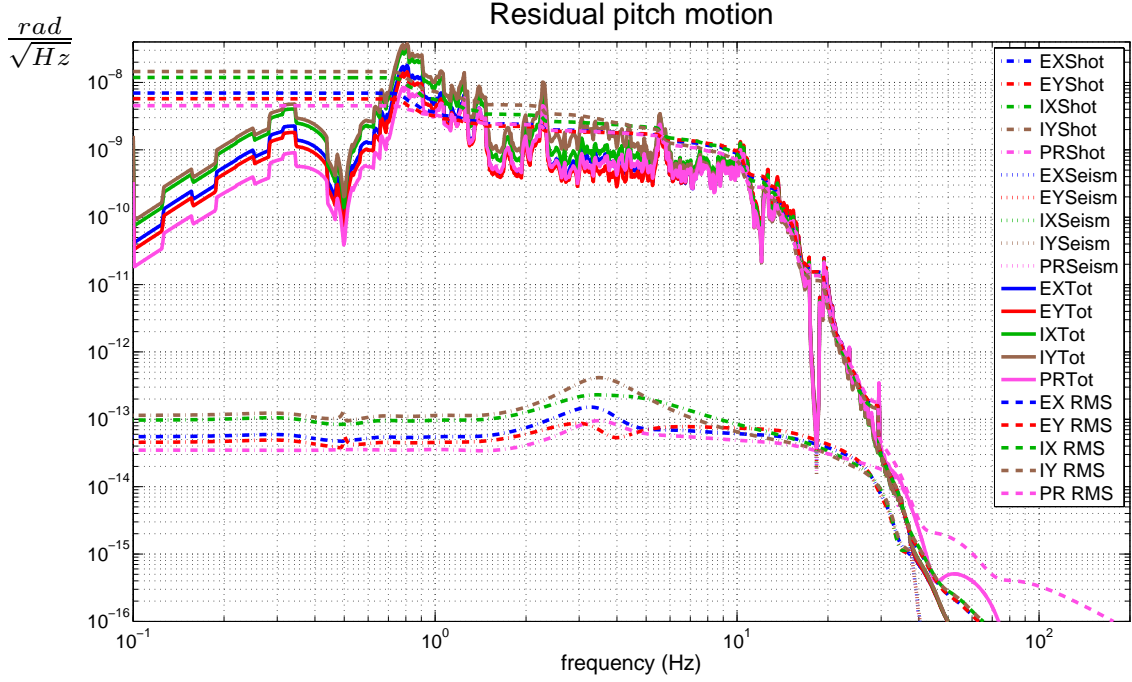
Figure 12: Residual angular motion of the mirrors.

7 Angular noise: coupling to DARM

Angular fluctuations couple to the cavity length and in particular to the gravitational wave signal. In presence of a displacement of the beam with respect to the mirror rotation axis, a tilt of the mirror produces a phase shift of the beam which is equivalent to a length variation of the cavity. A way of quantifying the coupling is by taking the convolution of the beam spot motion on each mirror with the residual mirror motion (see figure 12 in previous section). For the end mirrors this approach is not valid, as we need to take into account the fact that the end mirror beam spot motion is dominated by the BS and input beam angular motion amplified by the cavity length. Under the assumption that the BS angular motion is described by the spectrum in figure 9), the RMS of the beam spot motion for the end mirrors is of the order of 1 mm and about a factor 10 smaller for the input mirrors (see figure 13).

The angular noise coupling to DARM is shown in figure 14. The plot shows that the source of angular noise below 50 Hz is the seismic noise, while above 50 Hz it is due to the noise of the sensors used for the angular control signals. The cut-off of the control filters is tuned in order to have the angular noise at least a factor 5 below the designed sensitivity starting at 50 Hz (see zoom of the previous plot in figure 15). There is room for more aggressive cut-offs, but some fine tuning is needed in order to keep the phase margin of the loops acceptable.
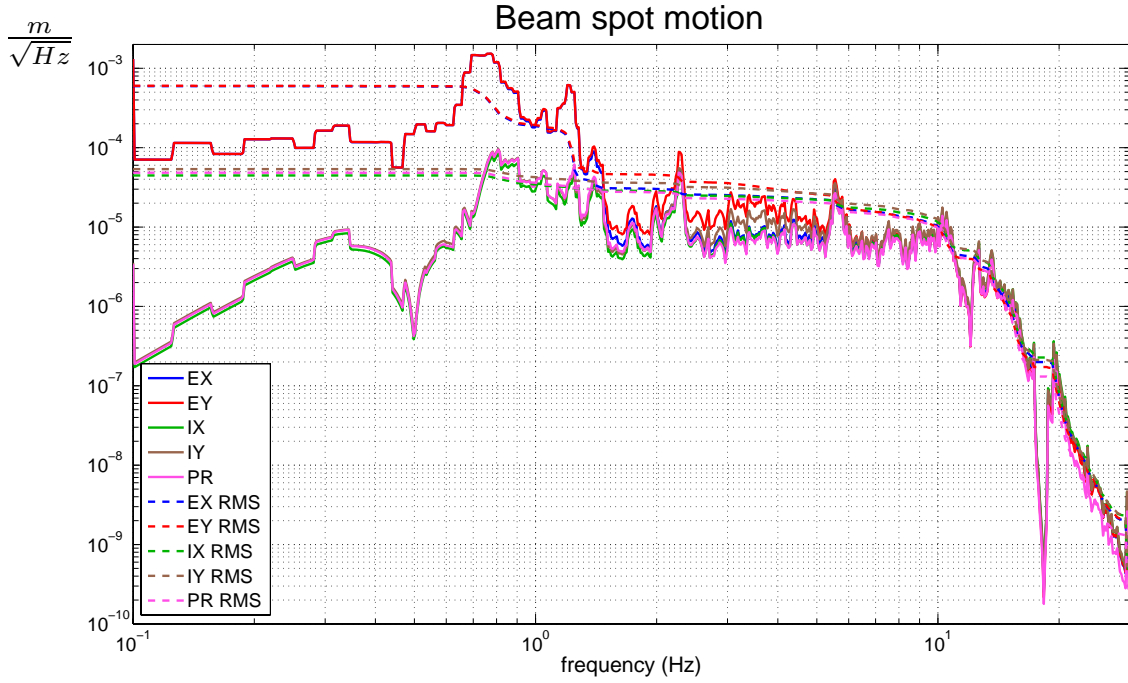
Figure 13: Beam spot motion of the mirrors. For the end mirrors the amplification due to the BS motion is considered. The resulting RMS of the beam spot motion of EX and EY is about 1 mm.
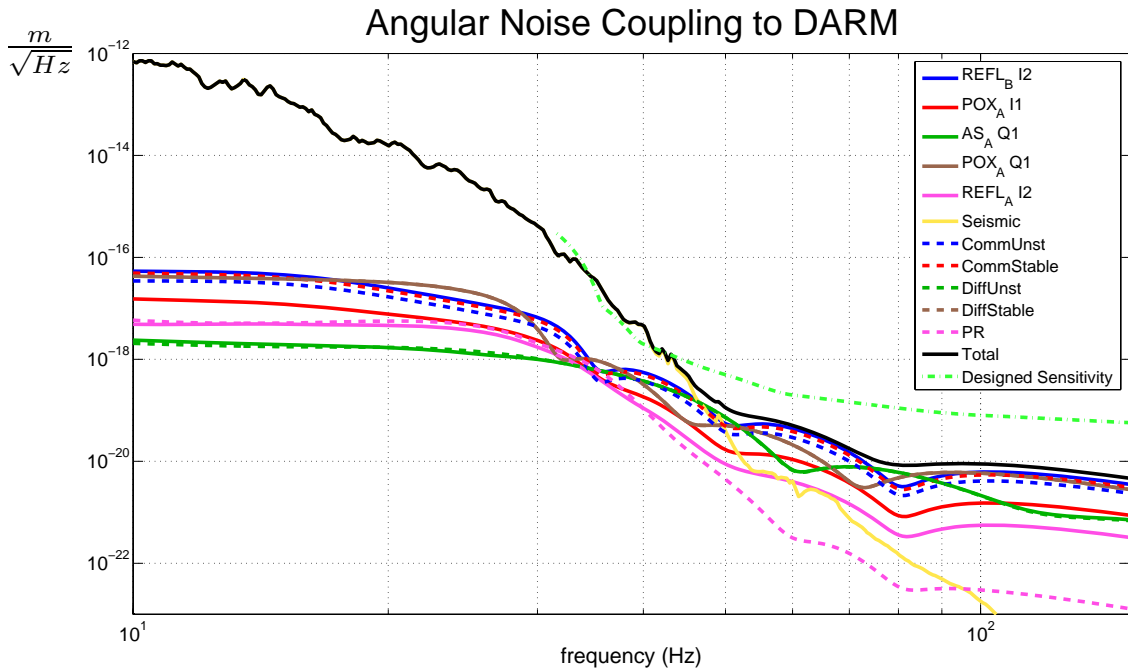

Figure 14: DARM noise induced by angular noise. The eLIGO designed sensitivity is based on [7].
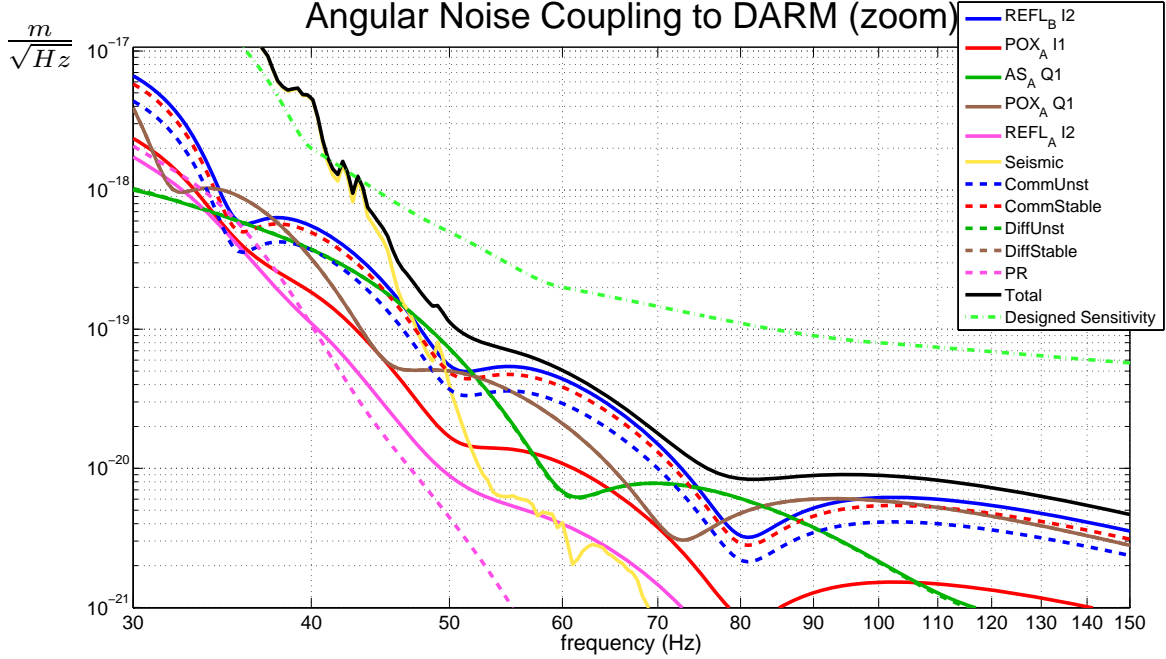
Figure 15: Zoom of the DARM noise induced by angular noise.

8 Conclusion

Radiation pressure effects significantly modify the mechanical transfer functions of the mirrors in eLIGO. An Optickle model has been used in order to study the controllability of the angular degrees of freedoms and the angular noise coupling to the dark fringe. There is a preferred mirror basis, corresponding to the stable and unstable modes of the arm cavities, in which the matrix of the mechanical transfer functions is diagonal, and the diagonalization is frequency and input power independent.

In this basis, a scheme which uses WFS signals detected at the REFL, POX and AS ports is sufficient to control the 5 angular degrees of freedom of the IFO. The bandwidth of the unstable control loops needs to be as high as possible in order to have enough gain at low frequency to reduce the mirror motion, and at the same time prevent multiple unity gain crossing in the open loop transfer function.

With seismic noise and shot noise included in the model, the angular noise coupling to the dark fringe is dominated by the unsuppressed seismic motion of the mirrors below 45 Hz. By assuming shot noise limited WFSs with 1 mW impinging power, the shot noise of the sensors is the limiting noise source above 45 Hz. According to this model, starting from 50 Hz the angular noise can be made at least a factor 5 below the designed eLIGO sensitivity.

A   Appendix: Sensing matrix at LLO

The alignment sensing matrix measured at LLO [4] is shown in table 8. The measurement has been taken at 10 Hz, with 2.8 W of power entering the IFO and DARM locked on DC with 20pm offset. The matrix is in the mirror base, and the demodulation phase of the signals is tuned with respect to the common and differential mirror base.

	ETMX	ETMY	ITMX	ITMY	RM
REFL_B I2	2620.0	2174.5	26.0	-71.5	8054.6
REFL_B Q2	1437.5	1188.9	-9.7	-58.2	4535.8
POX_A I1	727.4	302.8	-4721.9	-2805.4	16390.6
POX_A Q1	352.4	145.8	-4300.4	-1204.8	11014.7
AS_A I1	770.3	-595.6	-556.4	292.6	-118.5
AS_A Q1	-60045.1	55967.3	-25789.1	7927.9	21493.6
REFL_A I2	-79.6	126.0	192.6	111.4	-2460.7
REFL_A Q2	3.6	-38.3	-61.2	-25.4	374.4

Table 8: Sensing matrix measured at LLO, in the mirror base.

The basis has been changed to the stable and unstable one, and the demodulation phase of each signal has been optimized for that basis. The resulting matrix, after normalization, is shown in 9.

	CommUnst	CommStab	DiffUnst	DiffStab	PR
REFL_B I2	1	0.89	0	0	1.7
REFL_B Q2	0	0	0	0	0
POX_A I1	-0.67	1	-0.23	0.36	1.9
POX_A Q1	0	0	-0.13	0.13	0
AS_A I1	0	0	0	0	0
AS_A Q1	-0.13	0.10	-1	-0.46	0.15
REFL_A I2	-0.13	0.11	0	0	1
REFL_A Q2	0	0	0	0	0

Table 9: LLO sensing matrix with optimized demodulation phases for the stable and unstable basis.

A comparison with the sensing matrix computed in simulation 4 can not be directly done. The simulation in fact is not yet tuned so as to reproduce the WFSs location and the telescope in front of them. However, consistently with the simulation, the signals REFL_B I2, POX_A I1 and REFL_A I2 are mainly sensitive to the common dofs, where POX_A Q1 and AS_A Q1 are mainly sensitive to the differential dofs. As mentioned in section 4.1, no significative signal appears on AS_A I1, as expected.

B   Appendix: Alignment signals vs Gouy phases and demodulation phases

The RF amplitude-modulated alignment signal detected by each WFS can be written in the general form [6]:

$$\mathrm{WFS}(\eta, \Theta, \Gamma) = P_{in} f(\Gamma) f_{split} k_{PD} \times \sum_{i=1}^{5} A_i \Theta_i \cos{(\eta - \eta_i)} \cos{(\omega_m t - \phi_{Di})}$$

where the following notation is used:

P_{in} : input power;

Γ : modulation index, with $f(\Gamma) = 2J_0(\Gamma)J_1(\Gamma)(\approx \Gamma$ for $\Gamma \ll 1)$;

f_{split} : fraction of a particular port's light directed to the WFS;

k_{PD} : less than unity factor which accounts for the imperfection of the WFS geometry;

η : additional Gouy phase shift due to the longitudinal position of the WFS.

For the ith angular dof, the following parameters are also defined:

A_i : RF modulated component of the optical power due to the interference of TEM_{00} and TEM_{10} modes;

Θ_i : normalized misalignment angle;

η_i : Gouy phase between between TEM_{00} and TEM_{10} modes at the output port;

ϕ_{Di} : phase of the signal at the modulation frequency ω_m.

In order to study the sensitivity of the WFS signals to different dofs as function of Gouy phases and demodulation phases, it can be useful to consider a different representation of the WFS signal. For each port, let's consider the 4 dimensional space described by the I and Q phases of the two WFS, A and B:

$$\overrightarrow{sig}_{IN} = \begin{pmatrix} sA_I \\ sA_Q \\ sB_I \\ sB_Q \end{pmatrix}$$

These signals are frequency dependent, but for our purposes it is sufficient to consider the signal at a given frequency, so that the vector is just formed by 4 numbers. At each port, this vector can be used to represent the signal sensitivity at a given dof. We assume that the two

detectors are 90 degrees of Gouy phase apart and the signals have an initial demodulation phase of 0 degrees. In this space, a change of demodulation phase θ_d is represented by a rotational matrix like:

$$R(\theta_d) = \begin{pmatrix} \cos\theta_d & \sin\theta_d & 0 & 0 \\ -\sin\theta_d & \cos\theta_d & 0 & 0 \\ 0 & 0 & \cos\theta_d & \sin\theta_d \\ 0 & 0 & -\sin\theta_d & \cos\theta_d \end{pmatrix}$$

while a change of Gouy phase θ_g is given by a rotational matrix like:

$$R(\theta_g) = \begin{pmatrix} \cos\theta_g & 0 & \sin\theta_g & 0 \\ 0 & \cos\theta_g & 0 & \sin\theta_g \\ -\sin\theta_g & 0 & \cos\theta_g & 0 \\ 0 & -\sin\theta_g & 0 & \cos\theta_g \end{pmatrix}$$

After a θ_g change in the Gouy phase, and a θ_d change in the demodulation phase, the new

vector $\overrightarrow{sig_{OUT}} = \begin{pmatrix} sA'_I \\ sA'_Q \\ sB'_I \\ sB'_Q \end{pmatrix}$ is:

$$\overrightarrow{sig_{OUT}} = R(\theta_d) \times R(\theta_g) \times \overrightarrow{sig_{IN}}$$

whose components are:

$$sA'_I = +(\cos\theta_d\cos\theta_g)sA_I + (\sin\theta_d\cos\theta_g)sA_Q + (\cos\theta_d\sin\theta_g)sB_I + (\sin\theta_d\sin\theta_g)sB_Q \tag{B.1}$$

$$sA'_Q = -(\sin\theta_d\cos\theta_g)sA_I + (\cos\theta_d\cos\theta_g)sA_Q - (\sin\theta_d\sin\theta_g)sB_I + (\cos\theta_d\sin\theta_g)sB_Q \tag{B.2}$$

$$sB'_I = -(\cos\theta_d\sin\theta_g)sA_I - (\sin\theta_d\sin\theta_g)sA_Q + (\cos\theta_d\cos\theta_g)sB_I + (\sin\theta_d\cos\theta_g)sB_Q \tag{B.3}$$

$$sB'_Q = +(\sin\theta_d\sin\theta_g)sA_I - (\cos\theta_d\sin\theta_g)sA_Q - (\sin\theta_d\cos\theta_g)sB_I + (\cos\theta_d\cos\theta_g)sB_Q \tag{B.4}$$

The goal is to find a Gouy phase and demodulation phase rotation which maximizes the signal on one of the 4 components, for instance sA_I. In order to to that, let's zero the sA_Q and sB_I components, by solving the following system of equations for θ_d and θ_g:

$$sA'_Q = 0 \tag{B.5}$$

$$sB'_I = 0 \tag{B.6}$$

By adding the members of the equations together we find:

$$\tan \theta_g = -\frac{(sB_Q - sA_I)\sin\theta_d + (sA_Q + sB_I)\cos\theta_d}{(sB_Q - sA_I)\cos\theta_d - (sA_Q + sB_I)\sin\theta_d} \tag{B.7}$$

By combining equations B.7 with equation B.2, an expression for θ_d and θ_g in terms of the $\overrightarrow{sig_{IN}}$ components can be derived.

The two solutions are:

$$\overline{\theta_d} = \arctan\left(\frac{-\alpha + \sqrt{\gamma}}{\delta}\right) \qquad \overline{\theta_g} = \arctan\left(\frac{-\beta + \sqrt{\gamma}}{\eta}\right) \tag{B.8}$$

and

$$\theta_d = \arctan\left(-\frac{\alpha + \sqrt{\gamma}}{\delta}\right) \qquad \theta_g = \arctan\left(-\frac{\beta + \sqrt{\gamma}}{\eta}\right) \tag{B.9}$$

where the following parameters are defined:

$$\alpha = sA_I^2 - sA_Q^2 + sB_I^2 - sB_Q^2 \tag{B.10}$$
$$\beta = sA_I^2 + sA_Q^2 - sB_I^2 - sB_Q^2 \tag{B.11}$$
$$\gamma = 4(sA_I sA_Q + sB_I sB_Q)^2 + \alpha^2 \tag{B.12}$$
$$\delta = 2(sA_I sA_Q + sB_I sB_Q) \tag{B.13}$$
$$\eta = 2(sA_I sB_I + sA_Q sB_Q) \tag{B.14}$$

The first solution (equation B.8) gives the maximum absolute value of sA_I'.

An useful way of describing the signal, instead of using the vector $\overrightarrow{sig_{IN}} = \begin{pmatrix} sA_I \\ sA_Q \\ sB_I \\ sB_Q \end{pmatrix}$, is by means of 4 parameters:

- the amplitude of the signal (sA_I'),

- the orthogonal fraction of the signal (sB_Q'/sA_I'),

- the demodulation phase and the Gouy phase found in equation B.8, $\overline{\theta_d}$ and $\overline{\theta_g}$.

In summary, with two WFSs 90 degree Gouy phase apart at a given detection port, we can determine which are the Gouy phase and the demodulation phase rotations needed in order to maximize the signal on one phase of each WFS output.
Parameterizing our signal in terms of its amplitude, its orthogonal component and the Gouy phase and demodulation phase which maximize the signal amplitude, gives a more powerful representation than the I and Q components of the two WFSs at each port. In particular, this approach can be useful when dealing with experimental uncertainties in the Gouy phase measurement, or when studying the variations of the signal as function of the demodulation phase and Gouy phase tuning.

References

[1] Optickle is available in the MIT CVS repository at emvogil-3.mit.edu:/export/cvs/iscmodeling. The configuration file with the eLIGO parameters and the Optickle model used in this note can be found in the same place under the name "pickle".

[2] Sidles, Sigg *Optical torques in suspended Fabry-Perot interferometers*, Physics Letters A **354** (2006) 167-172.

[3] The analysis has been done by K.Kawabe on the LHO data. Details can be found in the eLIGO WIKI at http://lhocds.ligo-wa.caltech.edu:8000/mLIGO/ELIGO_ASC_Work_in_Progress.

[4] Measurements done by Kate Dooley at LLO on 7 July 2008. Details can be found in the eLIGO WIKI at http://lhocds.ligo-wa.caltech.edu:8000/mLIGO/ELIGO_ASC_Work_in_Progress.

[5] R. Adhikari *Sensitivity and Noise Analysis of 4 km Laser Interferometeric Gravitational Wave Antennae*, MIT, (July 2004).

[6] P. Fritschel et al. *Alignment of an interferometric gravitational wave detector*, Applied Optics, **37**, 28 (1998)

[7] R. Adhikari,P. Fritschel, S. Waldman *Enhanced LIGO*, LIGO internal note, LIGO-T060156-01-I (2006)